Exceptional multifunctionality in the feeding apparatus of a mid-Cambrian radiodont

Authors: Moysiuk, Joseph, and Caron, Jean-Bernard

Source: Paleobiology, 47(4) : 704-724

Published By: The Paleontological Society

URL: https://doi.org/10.1017/pab.2021.19

Paleobiology, 47(4), 2021, pp. 704–724
DOI: 10.1017/pab.2021.19

PALEOBIOLOGY
A PUBLICATION OF THE Paleontological SOCIETY

Article

Exceptional multifunctionality in the feeding apparatus of a mid-Cambrian radiodont

*Joseph Moysiuk** and *Jean-Bernard Caron*

Abstract.—Radiodonts (stem Euarthropoda) were ecologically diverse, but species generally displayed limited functional specialization of appendages along the body axis compared with crown group euarthropods. This is puzzling, because such functional specialization is considered to have been an important driver of euarthropod ecological diversification. One way to circumvent this constraint could have been the functional specialization of different parts of the frontal appendages, known to have been ecologically important in radiodonts. This hypothesis has yet to be tested explicitly. Here we redescribe the poorly known mid-Cambrian hurdiid radiodont *Stanleycaris hirpex* from the Burgess Shale (Stephen Formation) and quantitatively assess functional specialization of the frontal appendages of stem euarthropods. The appendages of *Stanleycaris* are composed of 14 podomeres, variously differentiated by their possession of pectinate endites, mono- to trifurcate medial gnathites, and outer spines. The oral cone is tetraradially organized and can be uniquely distinguished from those of other hurdiids by the presence of 28 rather than 32 smooth tridentate plates. Our phylogenetic analysis finds *Stanleycaris* in a grade of hurdiids retaining plesiomorphic raptorial appendicular functionality alongside derived adaptations for sweep feeding and large, bilaterally opposed gnathites. We conclude that the latter performed a masticatory function, convergent with gnathal structures like mandibles in various panarthropods. Taken together, *Stanleycaris* and similar hurdiids provide an extreme example of the evolution of division of labor within the appendage of a stem euarthropod and suggest that this innovation may have facilitated the functional transition, from raptorial to sweep feeding, at the origin of the hurdiid clade.

Joseph Moysiuk. Department of Natural History, Royal Ontario Museum, 100 Queen's Park, Toronto, Ontario M5S 2C6, Canada; Department of Ecology and Evolutionary Biology, University of Toronto, 25 Willcocks Street, Toronto, Ontario M5S 3B2, Canada. E-mail: joe.moysiuk@mail.utoronto.ca

Jean-Bernard Caron. Department of Natural History, Royal Ontario Museum, 100 Queen's Park, Toronto, Ontario M5S 2C6, Canada; Department of Ecology and Evolutionary Biology, University of Toronto, 25 Willcocks Street, Toronto, Ontario M5S 3B2, Canada; Department of Earth Sciences, University of Toronto, 22 Russell Street, Toronto, Ontario, Canada M5S 3B1. E-mail: jcaron@rom.on.ca

Accepted: 11 April 2021
*Corresponding author.

Background

Arthropods are unparalleled in their diversity of appendages, which are involved in almost every conceivable function—locomotion, sensing, feeding, respiration, grooming, mating, communication, defense, anchoring, and more. The ability to fulfill this wide range of requirements is considered to have been made possible in large part by an evolutionary capacity to partition functional tasks between different specialized appendages (Cisne 1974). This division of labor, or functional specialization, can circumvent trade-offs and is thus hypothesized to be selectively favored whenever the position of a specialized structure impacts its performance and as long as structural divergence is developmentally unconstrained (Rueffler et al. 2012). This in turn potentially opens opportunities for ecological diversification by allowing modular change in one functional attribute without compromising others.

A plethora of recent fossil discoveries suggest that a high level of morphological and ecological diversity had already been achieved among Cambrian euarthropods (Daley et al. 2018; Aria 2020). Given the complexity of

 0094-8373/21

Cambrian ecosystems (Caron and Jackson 2008; Zhao et al. 2014; Nanglu et al. 2020) and the marked appendicular differentiation seen among crown group euarthropods, functional specialization would also be expected to be plentiful in stem groups (sensu Jefferies 1979). However, in contrast to this prediction, differentiation of sets of appendages is generally more limited in stem euarthropods, as demonstrated by their relatively low "indices of tagmosis" on average compared with crown euarthropods (Cisne 1974; Wills et al. 1998; Yang et al. 2015). Do these differences represent a legitimate biological discrepancy, with stem groups being ecologically hyperspecialized relative to crown groups, or are they simply an artifact of the way functional diversity has been measured?

Radiodonta provides an exemplary test case. While phylogenetic placements outside the euarthropod total group or within the crown group were historically hypothesized, Radiodonta is now generally recognized as the most diverse clade of stem group euarthropods (|Daley et al. 2009, 2018). Radiodonts exhibit adaptations to a range of different feeding niches, from raptorial predation and durophagy to sediment sifting and suspension feeding (Whittington and Briggs 1985; Daley and Budd 2010; Vinther et al. 2014; VanRoy et al. 2015; Liu et al. 2018; Moysiuk and Caron 2019). Interestingly, this ecological diversification appears to have occurred via fairly limited morphological variations on a conserved body plan, characterized by a single pair of arthrodized frontal appendages followed by a series of relatively homonomous swimming flaps and sometimes rudder-like posterior blades and elongate furcae (Whittington and Briggs 1985; Chen et al. 1994; Daley et al. 2009; Cong et al. 2014; VanRoy et al. 2015; Moysiuk and Caron 2019). Much of the morphological divergence between the four major radiodont morphogroups—Anomalocarididae, Amplectobeluidae, Tamisiocarididae, and especially Hurdiidae—is concentrated in the appendages, illustrated by their broad dispersal in appendicular morphospace (Aria and Caron 2015), acknowledging the caveat that a number of species are known from only appendicular remains. If radiodont ecological diversification was not largely achieved by alteration of the tagmatic partitioning of functional roles, we hypothesize that differential functional specialization of parts of the frontal feeding appendages, enabling appendage multifunctionality, could have provided a partial substitute.

As a relevant case study, we contribute a redescription of the feeding apparatus of the mid-Cambrian hurdiid radiodont *Stanleycaris hirpex*, based on exceptionally preserved fossils from the Burgess Shale. Since the discovery of *Stanleycaris* (Caron et al. 2010) a decade ago, a large amount of new radiodont fossil material has contributed immeasurably to knowledge of this group of animals (e.g., Daley and Bergström 2012; Daley et al. 2013a,b; Cong et al. 2014, 2017; Vinther et al. 2014; VanRoy et al. 2015; Guo et al. 2018; Liu et al. 2018; Moysiuk and Caron 2019). In light of these advances, along with new *Stanleycaris* appendages and mouthparts collected from the Burgess Shale, we here revisit the morphology of this taxon. Armed with these data, we undertake a quantitative assessment of the evolution of functional diversity of radiodont appendages.

Systematic Paleontology

Superphylum Panarthropoda Nielsen, 1995
Order Radiodonta Collins, 1996
Family Hurdiidae Lerosey-Aubril & Pates, 2018
Genus *Stanleycaris* Pates et al., 2018, ex Caron et al., 2010

Emended Diagnosis and Description.—As for species.

Stanleycaris hirpex Pates et al., 2018, ex Caron et al., 2010

Locality and Stratigraphy.—"Thin" Stephen Formation of Stanley Glacier (Caron et al. 2010) and northern Tokumm Creek (Mayers et al. 2018), British Columbia, Canada. All material is housed at the Royal Ontario Museum, Invertebrate Palaeobiology Section (ROMIP), in Toronto, Canada (see list in Supplementary Material). This taxon is probably also present in the Wheeler Formation of Utah, USA (Pates et al. 2017).

Emended Diagnosis.—Hurdiid radiodont with the following characteristics: appendage with 14 podomeres, including proximal peduncle. Mesially curving, bladelike endites on

second to seventh and ninth podomeres, with proximalmost endite inclined more distally than subsequent ones and distalmost endite reduced in size. Enditic auxiliary spines short, numbering two to six. Medial gnathites of appendage large with one to three long, inward curving spines. Oral cone comprising four large tridentate plates with paired triangular nodes separated by sets of six smaller tridentate plates. Inner oral plates absent.

Preservation.—Pairs of appendages and oral cones in close proximity suggest a residual cuticular connection between these structures such that they remained associated after transport and burial (Fig. 1). The occurrence of multiple radiodont appendages on individual bedding surfaces has been reported previously from the Burgess Shale in *Anomalocaris* (O'Brien et al. 2014) and *Cambroraster* (Moysiuk and Caron 2019) and may evince gregarious molting behavior followed by rapid burial. A mass molting event would also be consistent with evidence for flexible deformation of appendicular spines (Figs. 1C, 2E) facilitated by the softening of the cuticle during ecdysis.

The appendages had a complex three-dimensional geometry such that no single orientation of burial shows all features. Typically, they are preserved with a strongly convex outer margin, with the distal end almost completely recurved relative to the proximal end (Figs. 2F,G, and 3A,G,H); however, some specimens are approximately straight (Fig. 1E). This suggests that nearly 180° of tip flexure was possible, with the distal five podomeres appearing particularly articulable. A second aspect of curvature is also evident when comparing appendages preserved at different angles. Moving distally, the appendage twists such that the distal tip lies slightly medial to the proximal end and can articulate to oppose the mesially curving endites.

Stanleycaris oral cones are also preserved in a variety of orientations and in variable states of disarticulation (Figs. 1A–E, 3). The more sclerotized oral margins of the plates may be the only remnants in some cases (Fig. 3G–I).

Description.—Appendages range in size from 3.5 to 32.2 mm, measured along the curving outer margin (figured and referred specimen table, Supplementary Material). They consist of 14 podomeres, which taper gradually toward the distal end of the appendage (Fig. 2). The first two proximal podomeres are more elongate (1.3–2.5 times longer) than subsequent podomeres (Figs. 2A,C,J, and 3A). The first in particular tends to be more variably preserved and less consistent in shape along the proximal margin. This suggests that it was less sclerotized than more distal podomeres and may have afforded limited flexibility, assisting with basal movement of the appendage. The following podomeres are subrectangular to subtrapezoidal (ca. half as long as tall) and may possess up to three spinous cuticular outgrowths on the inner, medial, and outer surfaces (Fig. 2). The distalmost podomere consists of a terminal spine, about 0.15 times the height of the first podomere (Fig. 2E,H,K).

The inner outgrowths (endites) are the most conspicuous and occur on podomeres 2–7 and 9 (Fig. 2A–F), and we number them according to the respective podomeres. They are blade-like, a third as wide as the length of the supporting podomeres. Each endite appears to be slightly crescentic in cross section, such that at some burial orientations the narrow edges may be juxtaposed on the bedding plane, producing a high-relief axial line, giving the appearance of a double edge (Figs. 1A–C, 2F, J, and 3G,H). The endite on the second podomere projects toward the distal end of the appendage, medial to the more distal endites (Figs. 1A–C, and 2A–C,J). It is about as long as the height of the supporting podomere. The endite on the third podomere projects roughly perpendicular to the supporting podomere and is about 1.7 times as long (Fig. 2A,C). Endites on the fourth to seventh podomeres are inclined distally at progressively more acute angles, resulting in their orientation roughly in parallel or slightly converging when the appendage is in its most common state of gentle flexure (Fig. 2A,C). These endites maintain their relative size ratio with respective supporting podomeres, decreasing slightly in absolute length distally, but because of the curvature of the appendage axis, their tips converge when the appendage is fully flexed (Fig. 2F,J). The endite on the ninth podomere is the shortest of all (half the length of that on seventh podomere) and also projects roughly parallel to the

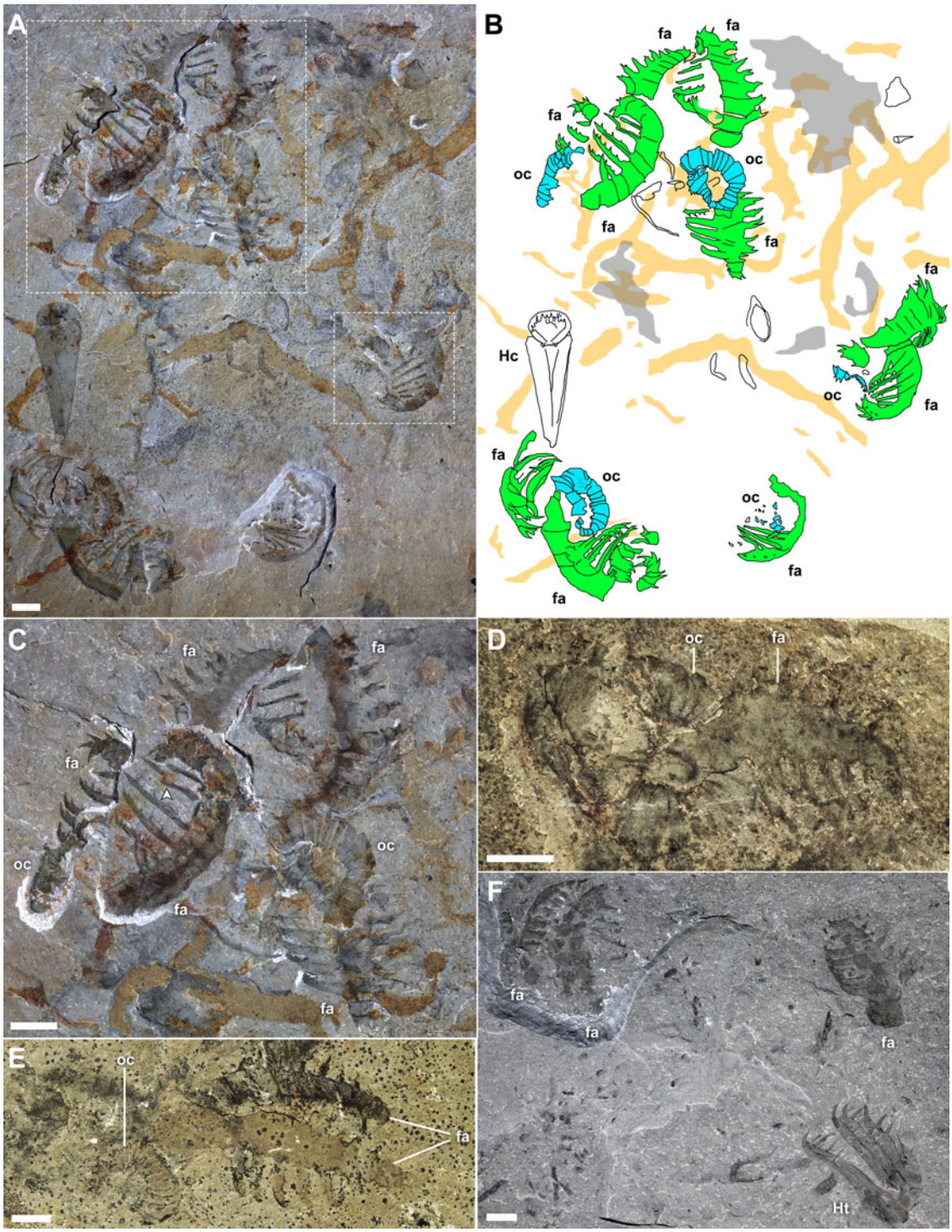

FIGURE 1. *Stanleycaris hirpex* assemblages. A–C, ROMIP 66118, assemblage slab representing at least five individuals; A, overview; B, line drawing, appendages and oral cones colored green and blue, respectively, burrows indicated in orange, organic stains in gray; C, close-up of upper boxed area in A, arrowhead indicating flexibly deformed endite; D, ROMIP 59976, isolated assemblage; E, ROMIP 59977, isolated assemblage; F, ROMIP 59975, *Stanleycaris* and *Hurdia* appendages preserved together. Abbreviations: fa, frontal appendage; Hc, *Haplophrentis carinatus*; Ht, *Hurdia triangulata*; oc, oral cone. Scale bars, 5 mm. (Color online.)

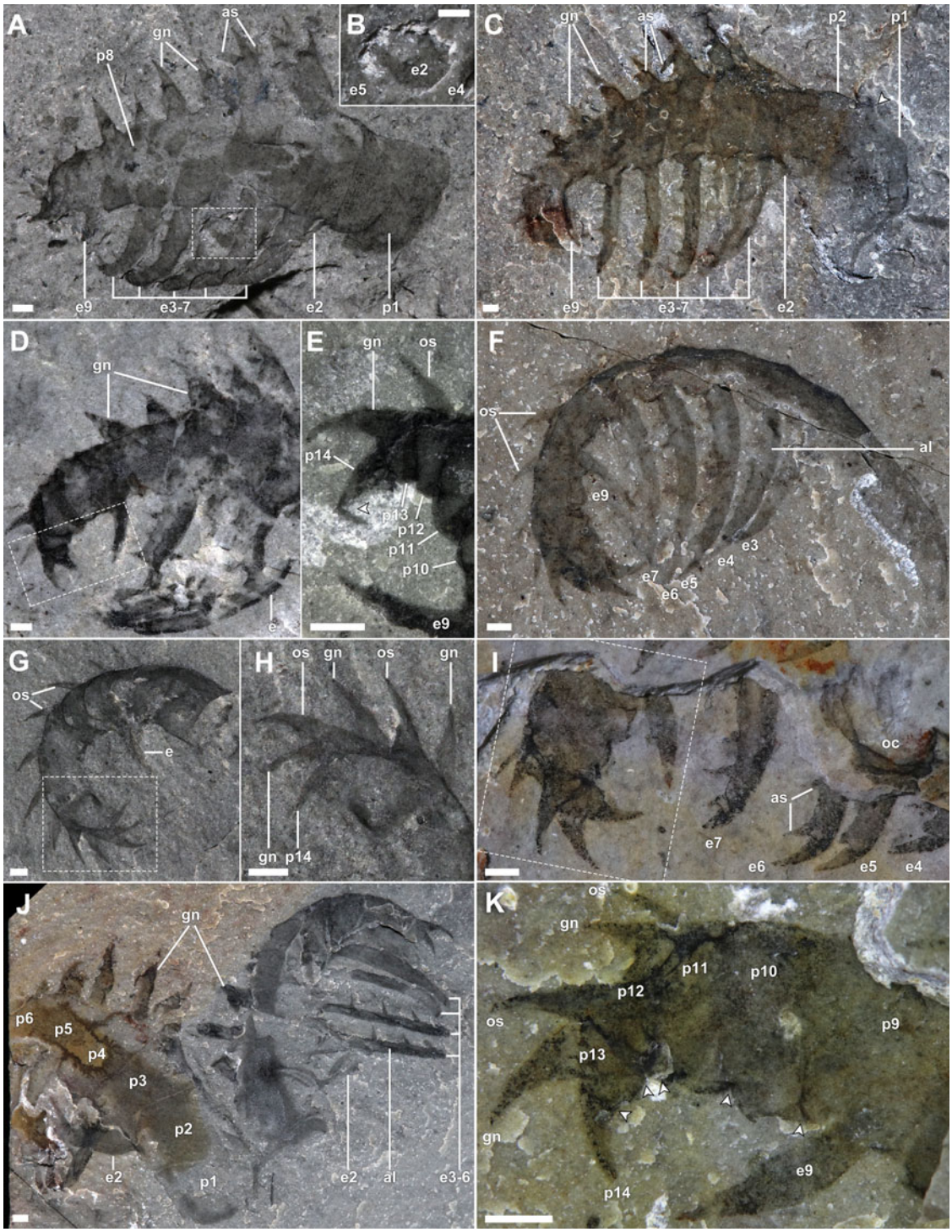

FIGURE 2. Morphology of *Stanleycaris* appendages. A, B, ROMIP 59975, isolated appendage, oblique lateral view; A, overview, fused part and counterpart; B, close-up of tip of proximal endite behind more distal endites; C, ROMIP 59944, Holotype, appendage in oblique lateral view, fused part and counterpart; D, E, ROMIP 66114, tilted appendage, showing distal podomeres; D, overview, fused part and counterpart; E, close-up of distal end; F, ROMIP 66119, appendage in ventral view, showing narrow profile of podomeres; G, H, ROMIP 66115, distal end of an appendage; G, overview, fused part and counterpart; H, close-up of distal podomeres; I, ROMIP 66118, appendage partly covered by matrix, overview; J, ROMIP 66117, pair of appendages, left one showing well-preserved proximal section; K, close-up of distal podomeres from I. Abbreviations: al, axial line on endite; as, auxiliary spine; e*x*, endite number (corresponding to p*x*); gn, gnathite; os, outer spine; p*x*, podomere number; other abbreviations as in Fig. 1. Scale bars, 1 mm.

more proximal endites (Fig. 2A,C–F,I,K). All endites display a strong mesial curvature and may appear shorter in oblique views as their distal tips curve into the matrix (Figs. 1E, 2A). Each endite bears a pectinate series of short auxiliary spines about 1.5 times the width of the endite, situated perpendicular to the endite long axis and projecting toward the distal end of the appendage (anterior surface; Figs. 1A–C, and 2C,I,J). Not counting the curving spinous termini of the endites, we interpret the number of auxiliary spines per endite as follows, from podomere 2 to 9: 3, 6, 5, 5, 4, 4, -, 2. Each auxiliary spine has a gentle medial curvature.

The medial spinous outgrowths of *Stanleycaris* occur on podomeres 3 to 13 (Figs. 2A,C–K, and 3A). We will refer to these structures here as gnathites (see "Evolution of Appendicular Functional Specialization"). The proximal gnathites are as long as the podomeres are high and 0.6 times as wide at the base—but they decrease in size distally until they are equivalent to the outer spines (described subsequently). Each consists of a main axial spine and may additionally possess an anterior (podomeres 6–9) or anterior and posterior (podomeres 3–5) auxiliary spines. The auxiliary spines splay away from the axial spine at an acute angle. The gnathites have overall a strong medial curvature. Because of this, the tips of the spines are often sharply folded over onto more proximal parts of the gnathite when the appendage is compressed mediolaterally (possibly exacerbated by flexible deformation in some cases; Fig. 2A,C). The curvature is most strongly developed in the anterior auxiliary spine, which is also slightly canted so that its tip is directed toward the distal end of the appendage.

The outer spines are simple, distally curving, and relatively small (Figs. 2,D–I,K, and 3A). Their length reaches 0.7 times the height of the supporting podomere distally. They are probably present from the 3rd to 13th podomeres, but they diminish in size proximally, such that those on the most proximal podomeres are difficult to distinguish. Particularly along the distal part of the appendage, these spines can be seen forming a row adjacent to that of the gnathites, but each row resides on a separate shale lamina. Podomere 13 is so short that its pair of spines project alongside the terminal spine, which is a similar size, together forming a distal trident (Fig. 2E,H,K).

The oral cone is tetraradially organized, with a large subsquare opening that is 0.4 times as wide as the total diameter (Figs. 1A–E, 3). Of the four large plates, the widest are positioned laterally, with slightly narrower plates at the anterior and posterior. Each of these is tridentate and additionally bears a pair of triangular nodes, slightly inset from the oral margin (Fig. 3E,F). Between the large plates are sets of six narrower plates (Figs. 1D, and 3C,D). These range from trapezoidal, adjacent to the large plates, to subrectangular in outline and from 0.7 to 0.4 times the maximum width of the large plates respectively. Their width along the oral margin is always less than half that of the large plates. Those in which the oral margin are well preserved also reveal three teeth (Fig. 3C–I). No inner plates are present within the oral cone. This is made clear by comparing one specimen in lateral view, preserving remains of the foregut (Fig. 3A,B), with a *Hurdia* oral cone (inner plates present) in similar orientation (Fig. 5G,H; also see Moysiuk and Caron 2019: fig. 2f,i).

Analytical Methods

Our Bayesian time tree makes use of an updated version (see matrix and character list, Supplementary Material) of the data matrix

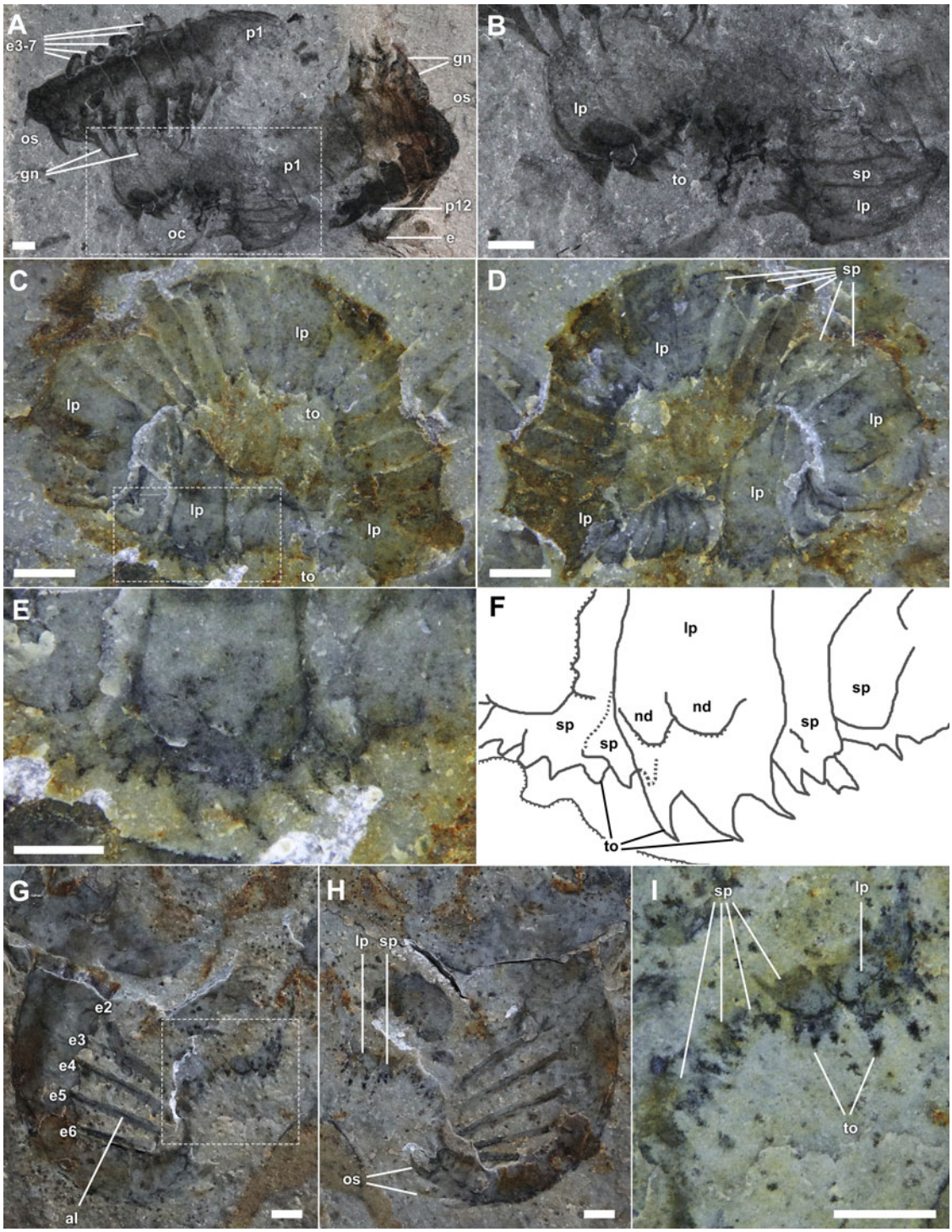

FIGURE 3. Morphology of *Stanleycaris* oral cone. A, B, ROMIP 66116, assemblage in frontal view consisting of a pair of appendages and oral cone; A, overview; B, close-up of oral cone; C–F, ROMIP 66118, obliquely oriented and overfolded oral cone showing sets of six small plates; C, D, overviews of part and counterpart; E, close-up of boxed region from C showing marginal teeth and nodes; F, interpretive drawing of E; G–I, ROMIP 66118, assemblage in lateral view; G, H, part and counterpart overviews; I, composite close-up of partially preserved plates with oral teeth. Abbreviations: lp, large oral plate; nd, node; sp, small oral plate; to, tooth on oral plate; other abbreviations as in Figs.1, 2. Scale bars, A–D, G–I, 2 mm; E, 1 mm.

published in (Moysiuk and Caron 2019), using the same substitution model (Mkv with neomorphic and transformational character partitions; Lewis 2001), a Strict clock model, and a Uniform tree model (Ronquist et al. 2012a) in MrBayes 3.2.6 (Ronquist et al. 2012b). *Hallucigenia+Ovatiovermis* was selected as an outgroup clade. The tree was tip calibrated using dates from the literature (references in character list in the Supplementary Material and Moysiuk and Caron [2019]), in light of recent updates to the Cambrian timescale (Karlstrom et al. 2020). For the root age, we employed a uniform prior from 550 to 537 Ma, as strongly supported by the compendium of fossil evidence (Daley et al. 2018). We selected a normal clock rate prior with mean 5×10^{-4}, SD 1×10^{-4} substitutions per site per Ma. Four runs were conducted for 5×10^{6} generations, sampling every 1×10^{3} generations, discarding the first 20% as burn-in. Convergence was verified in Tracer 1.6 (Rambaut et al. 2018).

To quantify the modular organization of frontal appendages in radiodonts and other taxa, we calculated the Brillouin diversity index for the various cuticular outgrowths (endites and outer spines) on the appendages of each species, similar to the previous application of this index to describe degree of tagmosis (Cisne 1974; Wills et al. 1998; Adamowicz et al. 2008; Yang et al. 2015). Coding was conducted by examination of fossil material housed at the Royal Ontario Museum and Smithsonian National Museum of Natural History (USNM), in Washington, D.C., as well as material figured in the literature. The outgrowths were grouped by similarity into sets, and the sum totals of each set were used to calculate the index (see Supplementary Material for a breakdown of the calculation for each species). Delimitation of outgrowths into sets was based on the identification of discontinuous variation in shape or size in adjacent outgrowths. Because this method, as previously noted, relies on somewhat subjective assessment of similarity, we also checked the sensitivity of our results to alternative coding schemes (Supplementary Material). *Zhenghecaris* was excluded, as its appendages are unknown. The resulting Appendicular Functional Specialization (AFS) index provides a proxy for the degree to which different regions of the frontal appendage were specialized to perform different types of functional tasks.

Once calculated, the AFS values were mapped onto the phylogeny, and maximum-likelihood ancestral state reconstruction was performed using the R package phytools (Revell 2012; R Core Team 2020). Corrected Akaike information criterion (AICc) model comparison was conducted with the *fitcontinuous* function in the package geiger (Harmon et al. 2008) using 1000 iterations each, resulting in decisive support for the Brownian Motion (BM) model over the White Noise model (ΔAICc = 28.32), and significant support for BM over the Ornstein-Uhlenbeck (ΔAICc = 2.27) and Mean Trend (ΔAICc = 2.28) models; BM results are reported in subsequent discussions.

Analytical Results

Our time tree topology (see "Evolution of Appendicular Functional Specialization") differs in certain aspects relative to analyses conducted with previous versions of this matrix using parsimony, maximum-likelihood, and uncalibrated Bayesian methodologies. The most important results are detailed below. A list of the characters supporting major clades can be found in the Supplementary Material.

Within Radiodonta, we find a polytomy of three major clades, corresponding to Hurdiidae (0.80 posterior probability), Tamisiocarididae (including *"Anomalocaris" saron*; 0.90), and a more heterogenous grouping of various "anomalocaridid" and "amplectobeluid" taxa

(0.55). Within Hurdiidae, a clade of all forms with large carapaces (0.60) is internally resolved, but found in a polytomy with *Stanleycaris*, *Schinderhannes*, *Peytoia*, and cf. *Peytoia*.

Lobopodians are generally characterized by zero AFS indices, with the exception of *Pambdelurion* and *Kerygmachela*, which have flagellate (presumably sensory) extensions distally on their frontal appendages. The limited but representative sampling of Cambrian euarthropods included in our tree likewise have zero AFS indices, whether or not the labrum is considered as their frontalmost appendage (Ortega-Hernández et al. 2017; Aria et al. 2020). *Surusicaris* has somewhat elevated AFS due to the differentiation of outer spines. By contrast, AFS indices in radiodonts are, with a few exceptions, notably elevated. Ancestral state reconstruction suggests a moderate increase in AFS at the origin of the radiodont clade, with subclades decreasing or increasing further subsequently. The highest values occur among the hurdiids, especially *Stanleycaris*, cf. *Peytoia*, and *Peytoia*, with an increase in AFS reconstructed at the base of the hurdiid clade. Moderately high values are also found in *Amplectobelua stephenensis* and *Laminacaris chimera*. The lowest values among radiodonts occur in *Caryosyntrips serratus*, *Tamisiocaris borealis*, *Cordaticaris striatus*, and *Aegirocassis benmoulai*; however, it should be noted that poor preservation of appendages in some of these could have resulted in underestimation of AFS, such that values should be interpreted with suitable caution. One alternative coding scheme, considering outer spines and distal gnathites in one group, had little overall qualitative effect, while another, omitting outer spines entirely, further emphasizes AFS in hurdiids relative to other taxa (Supplementary Fig. 1).

Radiodont Comparative Morphology

Our description (Fig. 4, Supplementary Video) reveals a more complex appendage structure than has been recognized in previous studies of *Stanleycaris* and provides the first detailed account of oral morphology (Caron et al. 2010; Pates et al. 2017). The combination of morphologies shared by other taxa emphasizes the evolutionary lability of the hurdiid appendage (Pates et al. 2019), perhaps related to interspecific differences in feeding ecology (see "Functional Implications").

Stanleycaris can be diagnosed most readily by the presence and large size of the medial spines (gnathites) and the unique pattern of endite occurrence. These characters also appear to be present in a single specimen described from the Wheeler Formation, supporting its identification as *Stanleycaris* (Pates et al. 2017).

Appendage: Endites.—As previously documented, the appendage of *Stanleycaris* bears characteristics of hurdiid radiodonts. The presence of five main bladelike endites is a key apomorphy for this group (Vinther et al. 2014; Moysiuk and Caron 2019). The inclination of the proximalmost endite is similar to the condition in *Hurdia* (Pates et al. 2019) and *Peytoia* (Fig. 5A–D). The presence of an intercalary podomere, lacking an endite, separating the proximal and distal portions of the appendage, is in common with *Cambroraster* and *Hurdia* (Moysiuk and Caron 2019). The enditic auxiliary spines of *Stanleycaris* are short, as in *Peytoia* and cf. *Peytoia* (Daley and Budd 2010) but are also fewer in number than in these forms.

Appendage: Gnathites.—The appendage of *Stanleycaris* is similar to *Peytoia* (Daley et al. 2013a) and cf. *Peytoia* (Daley and Budd 2010), sharing with these forms the large medial spines. We introduce here the term "gnathite" to refer to these structures, which are considered homologous with one of the rows of endites in non-hurdiid radiodonts (Vinther et al. 2014) but have migrated medially to the extent that they can no longer be appropriately termed "enditic." Use of the term "gnathite" is consistent with its usage to describe masticatory cuticular projections on euarthropod limbs (Haug et al. 2012; see "Functional Implications"). The gnathites of cf. *Peytoia* differ from those of *Stanleycaris* in possessing two auxiliary spines along the anterior margin and none along the posterior (Fig. 6F,G). The gnathites of *Peytoia* appear to be comparatively reduced and undivided (Fig. 5B). The Devonian *Schinderhannes* likely also possesses slender gnathites (Kühl et al. 2009), but poor preservation of the appendages prevents detailed comparison.

Gnathites may also be present outside the hurdiid clade. The distal reduction of the

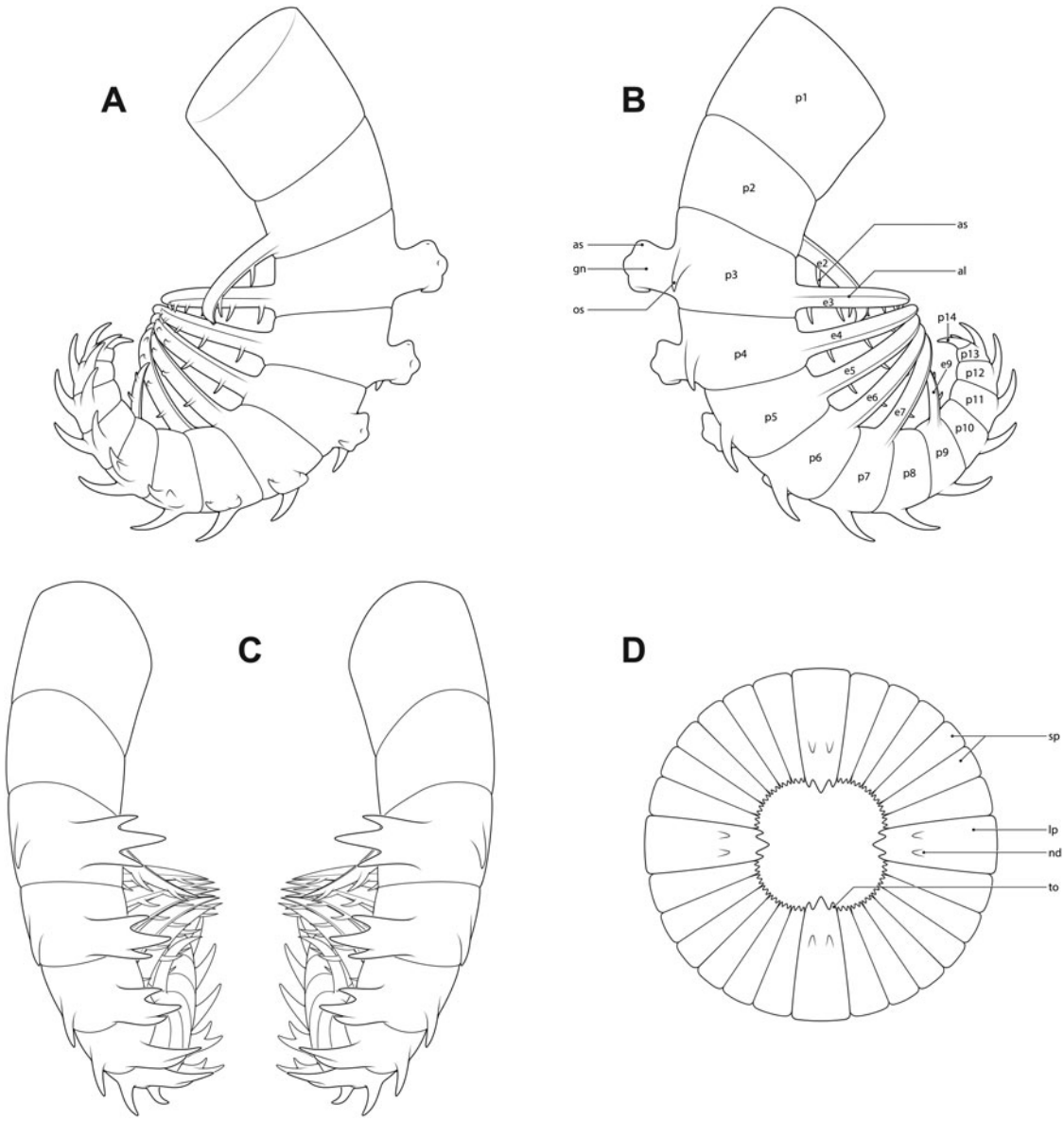

FIGURE 4. Appendages and mouthparts of *Stanleycaris hirpex*. A, Left appendage, medial view; B, left appendage, lateral view; C, pair of appendages, frontal view, showing the gnathal armature; D, oral cone. Abbreviations as in Figs. 1–3. Artwork by S. Cappelli.

endites and pairing of outer spines and gnathites in *Stanleycaris* is reminiscent of the paired spines visible near the distal outer margin in *Amplectobelua stephenensis* (Daley and Budd 2010; Fig. 5E,F). If the second pair of spines in *A. stephenensis* can likewise be interpreted as endite homologues that migrated to the medial side of the appendage (i.e., gnathites), this could represent a link between amplectobeluids and hurdiids (Moysiuk and Caron 2019); however, parallelism seems to be a more likely interpretation based on our present phylogenetic results. The position of the gnathites of *Stanleycaris* is also reminiscent of the condition in *Caryosyntrips*, although here the medially opposing spines are small, lack auxiliary spines, and are possibly paired (Daley and Budd 2010; Pates and Daley 2017).

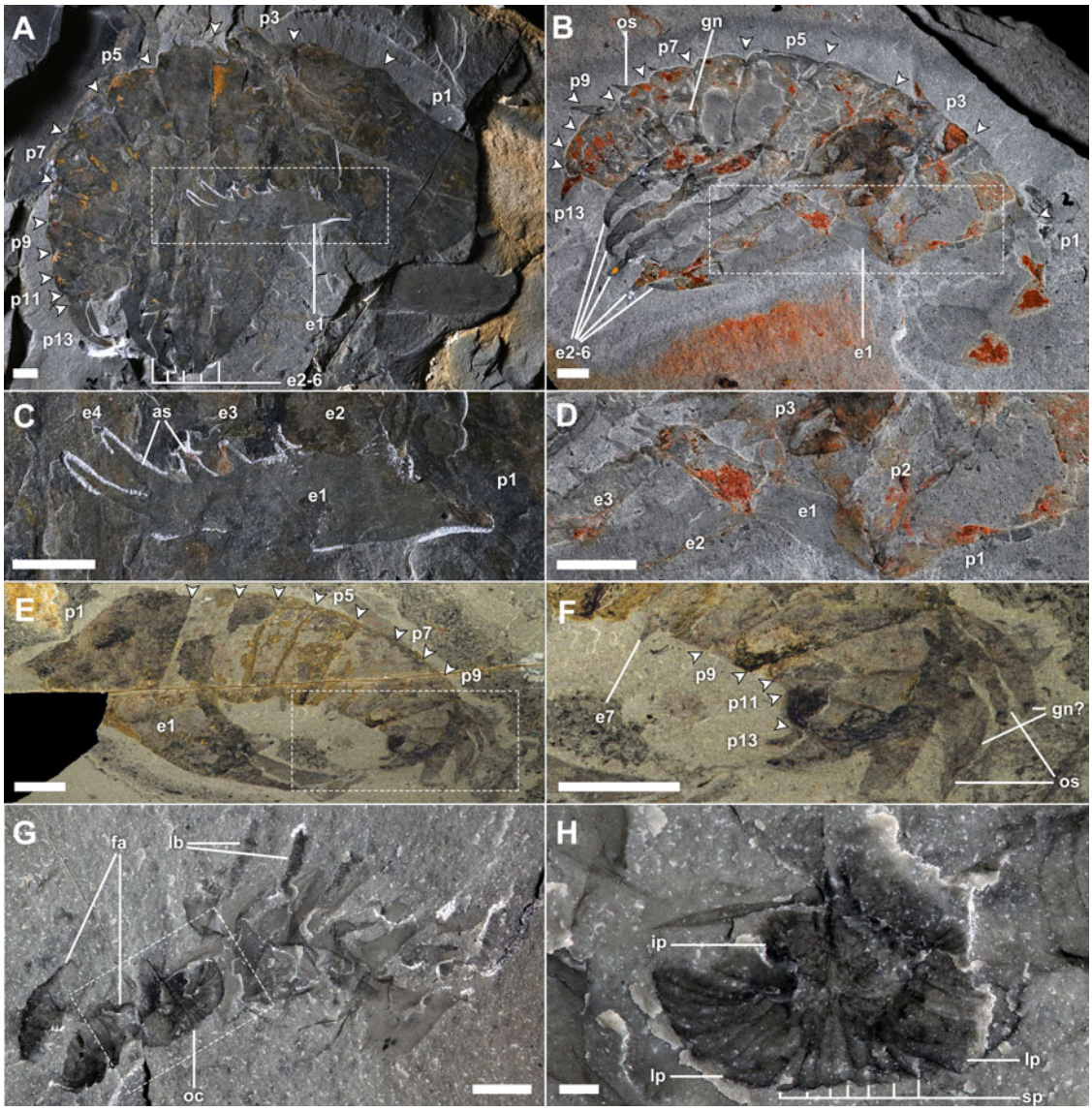

FIGURE 5. Radiodont comparative morphology. A–D, *Peytoia nathorsti* appendages; A, ROMIP 64257, overview, podomere boundaries marked with arrowheads; B, ROMIP 60043, overview, podomere boundaries marked with arrowheads; C, close-up of boxed region in A; D, close-up of boxed region in B; E, F, ROMIP 59492, *Amplectobelua symbrachiata* appendage, podomere boundaries marked with arrowheads; E, overview; F, close-up of boxed region in E; G, H, ROMIP 66120, *Hurdia triangulata* assemblage; G, overview of part; H, close-up of oral cone of counterpart with inner plate rows. Abbreviations: lb, lamellar bands; other abbreviations as in Figs. 1–3. Scale bars, A–G, 5 mm; H, 1 mm.

When compressed in a dorsal-oblique orientation, the podomere boundaries are diagonal to the appendage margins in *Stanleycaris*, which also resembles the situation in *Caryosyntrips* (Fig. 6B,E,F). *Caryosyntrips* has been consistently found in a polytomy with Radiodonta and Euarthropoda (Cong et al. 2014; Vinther et al. 2014; VanRoy et al. 2015; Lerosey-Aubril and Pates 2018; Liu et al. 2018); however, this result seems to be primarily due to the paucity of preserved characters in *Caryosyntrips*. The lack of other radiodont apomorphies (Supplementary Material) could instead be the result of secondary loss. Non-appendicular fossil discoveries may be critical to resolving this issue.

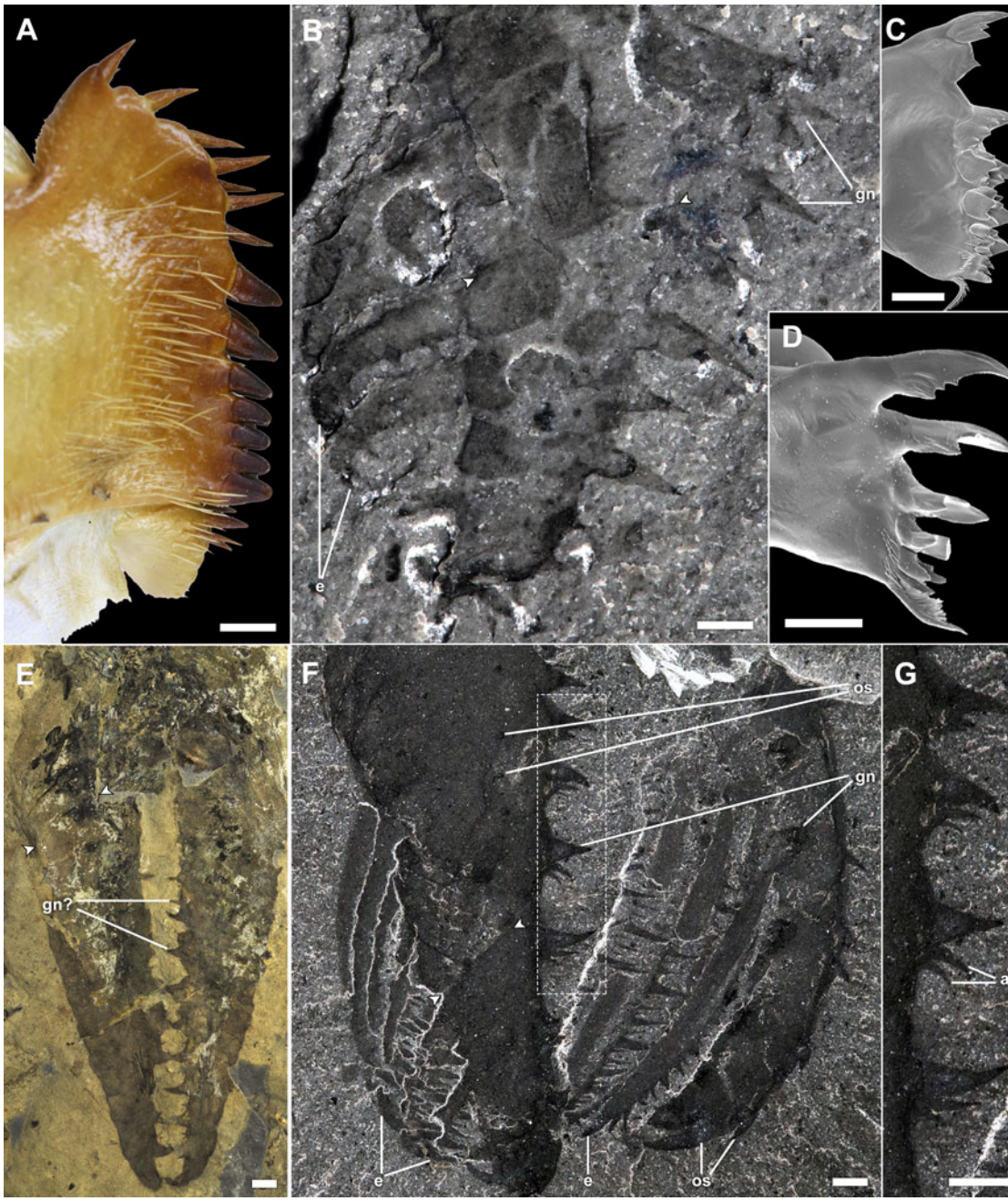

FIGURE 6. Gnathal convergence in radiodonts and euarthropods. A, Gnathobase of the xiphosuran *Limulus polyphemus*, courtesy of R. Bicknell; B, ROMIP 59975, frontal appendage of *Stanleycaris hirpex*; C, mandibular gnathobase of the durophagous copepod *Calanus propinquus*, courtesy of J. Michels; D, mandibular gnathobase of the predatory copepod *Paraeuchaeta antarctica*, courtesy of J. Michels; E, ROMIP 59501, frontal appendages of *Caryosyntrips serratus*; F,G, USNM 57490, frontal appendages of cf. *Peytoia*; F, overview showing opposing gnathites; G, close-up of gnathites. Abbreviations as in Figs. 1–3. Arrowheads indicate one angular podomere boundary. Scale bars, A, B, E–G, 2 mm; C, D, 50 μm.

The gnathites of *Stanleycaris* also resemble the endites of *Anomalocaris canadensis* in their trident-like shape (Daley and Edgecombe 2014); however, they are set apart by their curvature and attachment along the outer-medial rather than the inner margin of the

appendage. In curvature, the gnathites of *Stanleycaris* more closely resemble the toothed margins of the oral cone, which could point to functional similarities (see "Functional Implications").

Distal End of the Appendage.—*Stanleycaris*, *Peytoia*, and cf. *Peytoia* also share a robust and multisegmented distal portion of the appendage, resembling the raptorial ends of anomalocaridid and amplectobeluid appendages (Daley and Budd 2010; Moysiuk and Caron 2019). Other hurdiids with this characteristic include an unnamed hurdiid appendage from the Fezouata Formation (Van Roy and Briggs 2011) and *Ursulinacaris grallae* (Pates et al. 2019). Comparisons with these forms are hindered by the limited material available, but see "Note on *Ursulinacaris*." The distribution of multisegmented distal regions of the frontal appendage in amplectobeluids, anomalocaridids, tamisiocaridids, and early-diverging hurdiids points to retention from a common ancestor.

Note on Ursulinacaris.—*Ursulinacaris* was recently described as possessing narrow, paired endites. This contrasts with the condition in all other hurdiids, in which one set of endites is broad and the other has either been modified into medial gnathites (as in *Stanleycaris*) or lost altogether (e.g., *Cambroraster*) (Vinther et al. 2014; Moysiuk and Caron 2019), and was suggested to provide a link with tamisiocaridids (Pates et al. 2019). We note, however, that the structures interpreted as paired endites consist of lighter-colored, parallel marginal areas flanking a darker axial lineation, with no clear evidence of interspace. This resembles the specimens of *Stanleycaris* described earlier (Figs. 2F,J, and 3D,E), but here demonstrably only a single row of broad endites is present. In *Stanleycaris*, we interpret the dark axial lineation as the tapered edge of the single bladelike endite and the occasional preservation of a "doubled" margin with two layers of cuticle as a consequence of the juxtaposition of the two narrow edges during compression. We think this interpretation likely holds for *Ursulinacaris* as well. By contrast, if a second set of endites were present in *Ursulinacaris*, we would expect to see them clearly and divergently spaced apart from the first, as in other taxa (Daley et al. 2013b; Daley and Edgecombe 2014; Vinther et al. 2014).

Ursulinacaris resembles cf. *Peytoia* in terms of the number and position of endites and inclination of the proximalmost endite. While it differs in the apparent lack of gnathites, these might simply be hidden due to burial orientation, as seen in specimens of *Stanleycaris* (e.g., Figs. 2F, and 3D,E). New fossil material will be needed to assess the phylogenetic significance of *Ursulinacaris*.

Implications for Alignment of Podomeres in the Radiodont Appendage.—The appendage of *Stanleycaris* raises the issue of homologous alignment of podomeres in the radiodont appendage. Radiodont appendages have been terminologically divided into two parts: a proximal peduncle and a distal articulated portion (Guo et al. 2018). While the number of podomeres varies, a distal section composed of 13 podomeres is by far the most common (Pates and Daley 2017; Guo et al. 2018; Figs. 5D,E, and 7), and based on the phylogenetic distribution of this configuration, it is likely to be ancestral for radiodonts as a whole (see Supplementary Material). Among non-hurdiids, this stability is broken only by a few taxa that have evolved autapomorphic increases in podomere number (Wang et al. 2013; Vinther et al. 2014) and by *Lyrarapax*, which has decreased the number to 12 (Liu et al. 2018). The shortened appendages of many hurdiids represent a departure from other radiodonts, contributing to their differentiation in morphospace (Aria and Caron 2015) and challenging homology determination for structures in hurdiid relative to non-hurdiid appendages.

Here, our redescription of *Stanleycaris* contributes some insight. The similar pattern of a differentiated proximalmost ("shaft") endite followed by five similar elongate endites in *Stanleycaris* and other hurdiids provide a clear basis for homologous alignment within this clade (Pates et al. 2019). *Stanleycaris* is unique, however, in possessing an additional podomere proximal to the one bearing the proximalmost endite (we reject the interpretation of a similar podomere in *Hurdia*, reported questionably in a single specimen in Guo et al. [2018] and Pates et al. [2019], in favor of the original interpretation from Daley and Budd [2010] and Daley et al. [2013a]). Interpreted under the prevailing alignment hypothesis, the two

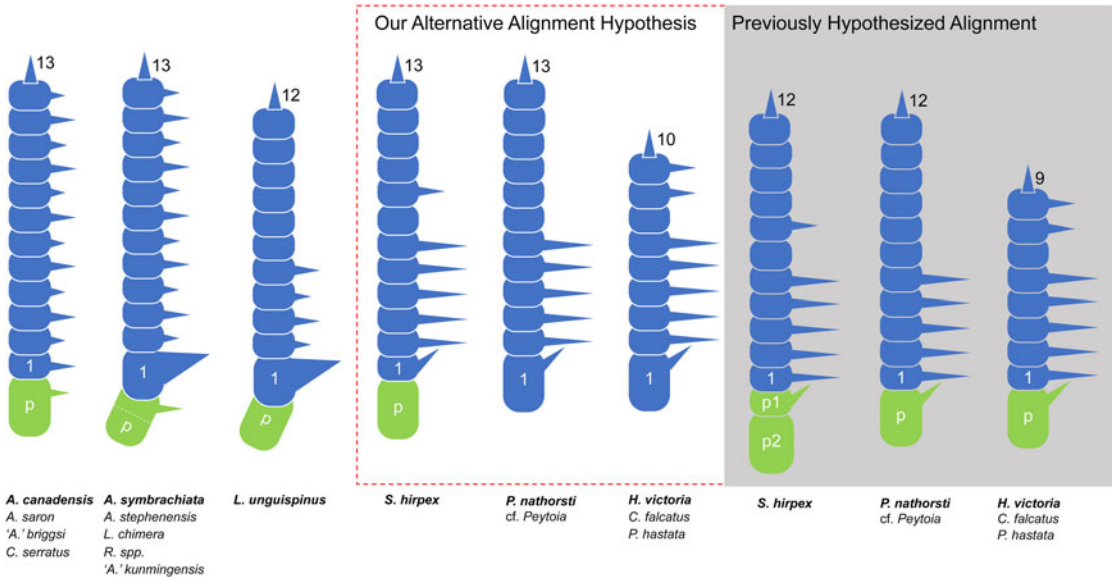

FIGURE 7. Hypotheses of radiodont frontal appendage podomere homology. Simplified diagrams of radiodont appendages contrasting the hypothesis for the alignment of hurdiid with non-hurdiid appendages favored in this paper with that suggested in, e.g., Guo et al. (2018) and Pates et al. (2019). Outer spines, second endites/gnathites, and auxiliary spines omitted for clarity. Peduncle is labeled p (light green), while distal podomeres (blue) are numbered starting at the podomere adjacent to the peduncle (1). Species in bold are represented, with other similar species listed below. Podomere counts are based on examination of fossil material housed at the ROM (*Stanleycaris hirpex*, *Peytoia nathorsti*, cf. *Peytoia*, *Amplectobelua stephenensis*) and in the published literature (Pates and Daley 2017; Guo et al. 2018). We interpret the articulated terminal spine observed in *Amplectobelua symbrachiata* (Cong et al. 2017: "ts" in their fig. 2) as the 13th podomere, and our reexamination of fossil material of *A. stephenensis* finds the corresponding 13 podomeres (Fig. 5E,F). Based on the figured material, we think the same is also likely the case for *"Anomalocaris" kunmingensis* (Wang et al. 2013; Liu et al. 2018). (Color online.)

proximal podomeres of the *Stanleycaris* appendage would both be considered part of a subdivided peduncle (Fig. 7). However, we think that this alignment may not be optimal for two key reasons, as follows.

First, it has been controversial as to whether various linear traces within the peduncle in some species are indeed segmental articulations rather than annulations, cuticular folds, or taphonomic artifacts (Lerosey-Aubril and Pates 2018). The most compelling case for a multipodomerous peduncle comes from *Amplectobelua symbrachiata* (Cong et al. 2017), but even here the expression of the putative boundaries is somewhat variable. In other species, the peduncle is either composed of a single podomere (Daley et al. 2013b; Daley and Edgecombe 2014; Pates and Daley 2017) or we consider the number to be ambiguous (Cong et al. 2016, 2018; Guo et al. 2018). Thus, in the phylogenetic scenario in which the first two podomeres in the *Stanleycaris* appendage represent the peduncle, this subdivision would likely have to be interpreted as an autapomorphy.

Second, if we instead interpret only the proximalmost podomere of *Stanleycaris* as the homologue of the peduncle, then the distal articulated portion of the appendage is seen to consist of 13 podomeres, the probable ancestral number for radiodonts (Fig. 7). Under this alignment scheme the number of podomeres in *Peytoia* (Fig. 5A,B) and cf. *Peytoia* would also exactly match the 13 distal podomeres seen in most other radiodonts, reinforcing the notion of their phylogenetic divergence near the base of the hurdiid clade, with subsequent reduction in podomere number in derived forms like *Hurdia* and *Cambroraster* (Daley et al. 2013a; Moysiuk and Caron 2019). However, this would also imply that the proximal podomere of all hurdiids other than *Stanleycaris* would not be homologous with the peduncle of

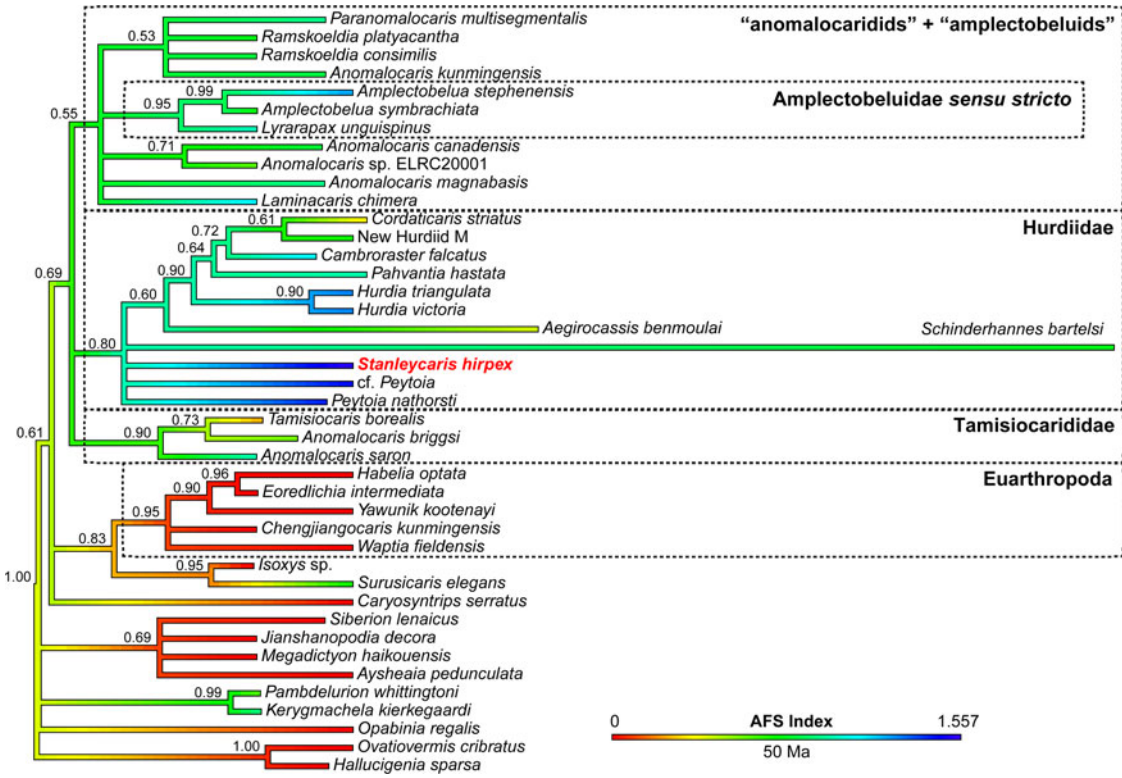

FIGURE 8. Evolution of early panarthropod frontal appendicular functional diversity. Cambrian panarthropod time tree (majority rule consensus), with maximum-likelihood ancestral state reconstruction of Appendicular Functional Specialization (AFS) index for frontal appendages. Numbers at nodes are posterior probabilities.

non-hurdiids, but rather with the first podomere of the distal articulated region, with the peduncle (or its distal articulation) being lost or not preserved (Fig. 7). Although both scenarios remain plausible, the one we present would seem to be more parsimonious.

Oral Structures.—While the appendages of *Stanleycaris* are distinctive, the oral cone (Fig. 4) is more typical. As in *Hurdia* (Whittington and Briggs 1985; Daley et al. 2013a) and *Cambroraster* (Moysiuk and Caron 2019), it is tetraradial with smooth plates bearing few teeth (sometimes with paired nodes on the large plates; e.g., Daley et al. 2013a: fig. 2f,j). The number of teeth per small circumoral plate differentiates *Stanleycaris* from at least *Hurdia*, in which two rather than three teeth are typically reported (Daley et al. 2013a). The lack of inner oral plates is comparable to the condition in oral cones identified to *Peytoia* (Daley et al. 2013a) and *Cordaticaris* (Sun et al. 2020). The most unusual feature in the *Stanleycaris* oral cone appears to be the presence of sets of six smaller circumoral plates, with seven being typical for hurdiids (Daley et al. 2013a; Moysiuk and Caron 2019; Sun et al. 2020) and probably for some amplectobeluids (Liu et al. 2018; Zeng et al. 2018). This presumably represents an autapomorphy for *Stanleycaris*, with an oral cone with 4 large and 28 small plates possibly being plesiomorphic for Radiodonta (Liu et al. 2018).

Interrupting the conservativism of radiodont oral cone morphology, Cong et al. (2017, 2018) observed disarticulated assemblages of *A. symbrachiata* and *Ramskoeldia* spp. with several sclerite types, leading them to hypothesize a radically different feeding apparatus. They speculatively reconstructed a four-sided complex of plates followed by three bilaterally paired, opposing "gnathobase-like structures" (GLS). In the context of this paper, this

hypothesis could imply a greater level of tagmatic functional specialization than other radiodonts, but the disarticulation of the material leaves an opening for alternative interpretations.

The GLS and other associated plates share similar ornamentation with oral plates of other radiodonts (Daley and Bergström 2012; Liu et al. 2018; Zeng et al. 2018). GLS differ primarily in being asymmetrical, with teeth curving to one side. We note that the circumoral plates of *Stanleycaris* and other taxa can become disarticulated, and the teeth on the large plates may sometimes appear to curve to the side in a similar way (Moysiuk and Caron 2019: fig. 2f,I; Fig. 3B,E). This is due to taphonomic deformation during oblique burial, with the orally directed teeth being deflected as the plate is compressed. Poor preservation of the proximal margins of the GLS is also shared with the oral plates in some specimens of *Stanleycaris* (Fig. 3G–I). Accepting the homology of circumoral plates and GLS opens the possibility that both are derived from structures belonging to multiple segments (Cong et al. 2019); however, this view conflicts with a phylogenetically deeper origin of circumoral sclerites, preceding segmentation itself (Smith and Caron 2015). Alternatively, we think that an organization of GLS, together with smooth and tuberculate plates, in a more typical radial oral cone remains plausible for *Amplectobelua* and *Ramskoeldia*.

Functional Implications

Multifunctionality and Convergence.—The suite of spinous outgrowths borne by the frontal appendages of *Stanleycaris* suggests a variety of different feeding functions. The basket-like array formed by the pectinate endites has been associated with sweep feeding, particularly with sediment sifting (Briggs 1979; Daley and Budd 2010; Moysiuk and Caron 2019). The relatively short endites and the sparse arrangement and stoutness of their auxiliary spines imply a much coarser fraction of food items could have been captured compared with microphagous forms like *Cambroraster*.

The multipodomerous distal end of the appendage of *Stanleycaris* lacks endites, except for the short one on the ninth podomere, which would have enabled considerable flexure. Flexing the distal end of the appendage would have brought the distally projecting spines into contact with the endites on more proximal podomeres. This is similar to the situation in raptorial feeders such as *Amplectobelua* (Chen et al. 1994) and *Lyrarapax* (Cong et al. 2014), although in *Stanleycaris* the flexure of the proximal end of the appendage would have been more impeded by the long proximal endites. Nonetheless, this morphology is suggestive of an ability for precise capture and manipulation of large and active prey (Liu et al. 2018).

The most distinctive aspect of the appendages of *Stanleycaris* is the row of gnathites, which oppose each other along the midline. Significantly, gnathites arise perpendicular to the plane of articulation of the podomeres, unlike the endites in anomalocaridids and amplectobeluids. This would have rendered it impossible for gnathites on the same appendage to interact, precluding raptorial functionality. Movement of the appendages within the plane of the gnathites could have been facilitated only through flexure at the base of the appendage, moving the entire distal arthrodized portion as a rigid structure (Whittington and Briggs 1985; Daley and Budd 2010; Moysiuk and Caron 2019). This would have brought the gnathites into occlusion with those on the opposing appendage. Simultaneous articulation of the podomeres might have added a slight perpendicular translation, producing a tearing and twisting motion (Whittington and Briggs 1985). This suggests that the pair of rigidly opposing gnathitic margins on the frontal appendages functioned together as a specialized jaw in *Stanleycaris*.

We regard the morphology and arrangement of the gnathites in medially opposing rows to be a striking example of proximate convergence (sensu Leander 2008) with paired opposing gnathal appendages in various panarthropods, in particular mandibles, but also to a lesser extent the multiple gnathobasic appendages of some arachnomorphs and the jaws of onychophorans (Fig. 6). In all cases, these appendages function together as a jaw, with rigid paired elements occluding along the midline to hold or masticate the food.

The form of jawlike elements is diverse among panarthropods (Manton 1964; Edgecombe et al. 2003). One of the most compelling comparisons can be made between the jaws of *Stanleycaris* and the mandibles of some copepods, which share a row of numerous large, multifurcate spines. In copepods, stout, pointed gnathobasic spines (Fig. 6C) concentrate force, enabling efficient cracking of biomineralized food items, while elongate, curving, bladelike spines (Fig. 6D) are associated with predation on large soft-bodied organisms (Michels and Schnack-Schiel 2005). By analogy, the curving, gracile gnathites of *Stanleycaris* appear best suited for holding, stabbing, and tearing soft-bodied prey. As noted earlier, *Peytoia*, cf. *Peytoia*, *Schinderhannes*, and *Caryosyntrips* share jawlike morphology with *Stanleycaris*. *Caryosyntrips* has been interpreted as a specialist durophagous taxon, using stout medial spines on its inflexible appendages to crack hard-shelled prey (Daley and Budd 2010; Pates and Daley 2017). Durophagy is also plausible for *Peytoia*, and particularly cf. *Peytoia*, whose gnathites are similarly stout (Fig. 6F,G). By contrast, the slender gnathites of *Schinderhannes* suggest a feeding preference closer to that of *Stanleycaris*. The differentiation of medial gnathites and their incorporation into rigidly opposing jaws therefore opened a range of feeding niches.

While we have drawn attention to notable similarities in morphology and function, the gnathites of *Stanleycaris* also differ in some ways from gnathobasic structures like mandibles. First, they are serially arranged on all distal podomeres instead of a single proximal one. A more comparable state has evolved in the postmandibular appendages of some extant and extinct mandibulates, which have subdivided protopods, each bearing a row of endites opposed along the midline that aid in processing food (Olesen 2007; Aria and Caron 2017; Vannier et al. 2018). This comparison cannot be taken further, however, as the endites project parallel to the plane of appendage articulation and more distal parts of the appendage (endopod) do not appear to be incorporated into the gnathal apparatus, contrary to *Stanleycaris*.

In addition, the feeding apparatus of *Stanleycaris* likely differed functionally from similar jaws in euarthropods. That the gnathites project perpendicular to the plane of articulation of the podomeres contrasts with the typical condition in gnathobasic jaws, where oppositional biting is performed by motion in plane with the jointing of the appendage, while shearing is accomplished by limited rotation at the base of the appendage, perpendicular to that plane (Manton 1964). Food particles broken up by *Stanleycaris*'s appendicular jaws could then have been channeled into the mouth by the mesially curving endites and perhaps further processed by the oral teeth. In crustaceans, an equivalent role is typically played by setose postmandibular appendages such as maxillae or maxillipeds (Watling 2015). Evolution of the unique feeding mechanism in *Stanleycaris* and similar taxa was presumably constrained by the orientation of their single pair of arthrodized feeding appendages, projecting anteriorly rather than laterally from the body.

Evolution of Appendicular Functional Specialization.—Many radiodont appendages consist of a series of homonomous podomeres, with differentiation provided only by the development of outer spines distally. The multifunctionality of the appendage of *Stanleycaris*, as well as *Peytoia* and cf. *Peytoia*, is outstanding in this respect, and accounts for their high AFS scores (Fig. 8), which are robust to variation in coding strategy (Supplementary Fig. 1). The reduction of distal endites in certain hurdiids (Daley et al. 2013a; Moysiuk and Caron 2019) and enlargement of a proximal endite in amplectobeluids (Hou et al. 1995; Liu et al. 2018) are other exceptions, manifest as modestly high values of AFS. However, these modifications appear to have contributed toward the singular feeding function of the appendage (sweep feeding and grasping, respectively) rather than partitioning diverse functional tasks between different appendage parts, and so cannot be viewed as multifunctionality in the same sense. Ancestral state reconstruction suggests that the high AFS in *Stanleycaris*, *Peytoia*, and cf. *Peytoia* represents the culmination of an increase that began in the common ancestor of the hurdiid clade. This result is found even with the inclusion of *Schinderhannes*, for which AFS may be underestimated, meaning that the actual increase along

the branch leading to Hurdiidae could have been greater.

The appendages of *Stanleycaris* and other early-diverging hurdiids suggest a plausible scenario for the evolution of the divergent sweep-feeding ecology characterizing this clade. The origin of the hurdiid-type appendage involved a drastic change in functional morphology, from a probable ancestral form, in which prey handling was accomplished by multiarticulatory raptorial grasping, to a derived state, in which oppositional basolateral sweeping became primary (Moysiuk and Caron 2019). However, the morphology of *Stanleycaris* and similar hurdiids demonstrates that this transformation did not occur wholesale. Rather, the increase in AFS at the origin of the hurdiid clade corresponds to the maintenance of plesiomorphic raptorial functionality at the distal end of the appendage, freeing other appendage modules to evolve novel sweep-feeding and gnathal adaptations. The decrease in AFS in some derived hurdiids would thus presumably correspond to subsequent ecological specialization via reversion to less functionally differentiated states.

This raises the question of whether evidence exists that other ecological shifts among radiodonts might have been facilitated by similar punctuational increases in AFS. While the paucity of known instances of such shifts hinders our ability to robustly test this hypothesis, our results do provide apparently contradictory cases. Ancestral state reconstruction suggests a decrease in AFS on the branches leading to *Aegirocassis* and *Tamisiocaris*, corresponding to hypothesized transitions to a suspension-feeding ecology (Vinther et al. 2014; Van Roy et al. 2015). Interestingly, the low AFS values observed in *Aegirocassis* and *Tamisiocaris* match the pattern of low tagmatic functional specialization observed previously in suspension-feeding euarthropods (Cisne 1974), suggesting that the possession of serial undifferentiated feeding structures might be a common theme for this guild. Unlike in the case of the hurdiids, these transitions to suspension feeding seemingly did not involve major reorganization of frontal appendage functional morphology, rather occurring via coordinated "global" increase in endite length and number of auxiliary spines, presumably enabling capture of increasingly small-sized prey. Given the less drastic nature of these morphofunctional changes, it is perhaps unsurprising that ecological transition was able to occur in the absence of a multifunctional transitional form. A similar case of integrated change in all endites may have occurred in the lineage leading to *Caryosyntrips*, although this is more ambiguous, considering the poor constraint on its phylogenetic position. Taken together, these cases suggest that a high level of AFS was not a prerequisite for ecological diversification among radiodonts, although it may have played a role in what was arguably the most spectacular transition at the origin of the hurdiid clade.

Radiodonts occupy the extreme high values in AFS relative to euarthropods and lobopodians. This may be in part an artifact of the dataset we employed, which includes only a highly limited (though phylogenetically representative) sampling of Cambrian euarthropods. Comparison of AFS values in a greater diversity of euarthropod taxa would be useful; however, controversy over the homology of radiodont and euarthropod frontal appendages (Cong et al. 2014; Aria et al. 2020) remains a notable constraint. Small sample size might likewise contribute to favoring of Brownian motion in our analysis, which otherwise seems at odds with the prediction of selection favoring functional specialization (Rueffler et al. 2012). Another factor is that AFS in this study considers only frontal appendages, and we would expect higher values of AFS in the postfrontal appendages of some euarthropods. A final caveat is that some types of functional specialization are not captured by our AFS metric, such as the multichelae and sensory flagellae formed by proximodistal subdivision of leanchoiliid endites (Aria et al. 2015). Thus, our results do not suggest that AFS in general was unimportant in the radiation of euarthropods, but they do conform with the hypothesis that frontal AFS was relatively important compared with tagmatic functional specialization in the diversification of radiodonts and that clade-specific patterns of functional specialization evolved in the context of the same Cambrian ecosystems.

While radiodont appendages vary considerably with their ecology, oral cone form is

more conserved, and how its function may have differed depending on feeding habits is a more open question. Speculatively, innovations like the inner oral plates present in some derived hurdiids (Daley et al. 2013a; Moysiuk and Caron 2019) could have provided release from functional trade-offs by compensating for the loss of masticatory gnathites on their frontal appendages, enabling more radical appendage specialization. Such oral modifications could thus have provided an alternative to appendicular functional specialization. The functional significance, if any, of other variations, such as the number of oral plates or presence of nodes or furrows on their surfaces, remains unclear (Daley and Bergström 2012; Zeng et al. 2018), in part due to the poor knowledge of oral morphology in most taxa. It will be useful to consider these aspects in future assessments of radiodont functional diversity as new fossil evidence comes to light.

Conclusions

In euarthropods, food capture and processing are typically performed by several specialized appendage pairs working in concert (Watling 2015). Radiodonts, constrained by the possession of only a single pair of arthrodized appendages, met similar imposed functional requirements either by adapting to relatively narrow feeding niches through integrated morphological change or by the evolution of increased functional specialization of different parts of the appendage. *Stanleycaris* is exemplary of the latter case, having appendages with strong differentiation of lateral–medial, inner–outer, and proximal–distal morphologies. This permitted appendage multifunctionality, including the ability to trap (endites), manipulate (distal raptorial portion), and masticate (gnathites) prey items. Multifunctionality may in turn have played a role as an evolutionary bridge between feeding ecologies in the ancestral hurdiid lineage, allowing dramatic niche diversification within the otherwise conserved radiodont body plan.

Bilaterally opposed jawlike appendages have evolved numerous times among panarthropods, most characteristically in the mandibles of mandibulates. We argue that *Stanleycaris* provides an equivalent example of evolutionary convergence in a Cambrian stem euarthropod. However, jaws in mandibulates, arachnomorphs, and onychophorans originate from different parts of the appendage (coxa, basipod, and distal claw, respectively; Boxshall 2004). *Stanleycaris* and similar radiodonts achieved convergence by even more divergent means, with whole appendages forming the opposing jaws. While convergence is often seen as a prime example of the long-term predictability of evolution (Blount et al. 2018), examples such as these underscore that convergent characters are mosaic products of both the ecological context that drives their evolution and the idiosyncrasies of the body plan in which they happen to emerge.

Acknowledgments

Fossils were collected by Royal Ontario Museum field parties under several Parks Canada Research and Collections permits to J.-B.C. and D. Collins. We thank S. Cappelli for artistic reconstructions; R. Bicknell and J. Michels for photos of the xiphosuran gnathobase and copepod mandibles, respectively; and M. Akrami and P. Fenton for assistance in the collections. J.M. also thanks A. Izquierdo López, J. Moon, and A. Daley for helpful discussions. Comments from J. Haug and one anonymous reviewer stimulated significant improvement of this article.

Major funding support for fieldwork comes from the Royal Ontario Museum (Research and collection grants, Natural History fieldwork grants), the Polk Milstein Family, the National Geographic Society (no. 9475-14 to J.-B.C.), the Swedish Research Council (to Michael Streng), the National Science Foundation (NSF-EAR-1556226, 1554897), and Pomona College (to Robert R. Gaines). This research was also indirectly supported by the Dorothy Strelsin Foundation (Royal Ontario Museum). J.M.'s doctoral research is supported by a National Science and Engineering Research Council (NSERC) Vanier Canada Graduate Scholarship through the University of Toronto (Department of Ecology and Evolution) and J.-B.C.'s NSERC Discovery Grant (no. 341944). This is the Royal Ontario Museum Burgess Shale project no. 89.

Data Availability Statement

Data available from the Dryad Digital Repository: https://doi.org/10.5061/dryad.kd51c5b5c.

Literature Cited

Adamowicz, S. J., A. Purvis, and M. A. Wills. 2008. Increasing morphological complexity in multiple parallel lineages of the Crustacea. Proceedings of the National Academy of Sciences USA 105:4786–4791.

Aria, C. 2020. Macroevolutionary patterns of body plan canalization in euarthropods. Paleobiology 46:569–593.

Aria, C., and J.-B. Caron. 2015. Cephalic and limb anatomy of a new isoxyid from the Burgess Shale and the role of "stem bivalved arthropods" in the disparity of the frontalmost appendage. PLoS ONE 10(6):e0124979.

Aria, C., and J.-B. Caron. 2017. Burgess Shale fossils illustrate the origin of the mandibulate body plan. Nature 545:89–92.

Aria, C., J.-B. Caron, and R. Gaines. 2015. A large new leanchoiliid from the Burgess Shale and the influence of inapplicable states on stem arthropod phylogeny. Palaeontology 58:629–660.

Aria, C., F. Zhao, H. Zeng, J. Guo, and M. Zhu. 2020. Fossils from South China redefine the ancestral euarthropod body plan. BMC Evolutionary Biology 20:4.

Blount, Z. D., R. E. Lenski, and J. B. Losos. 2018. Contingency and determinism in evolution: replaying life's tape. Science 362: eaam5979.

Boxshall, G. A. 2004. The evolution of arthropod limbs. Biological Reviews of the Cambridge Philosophical Society 79:253–300.

Briggs, D. E.G., 1979. *Anomalocaris*: the largest known Cambrian arthropod. Palaeontology 22:631–664.

Caron, J.-B., and D. A. Jackson. 2008. Paleoecology of the Greater Phyllopod Bed Community, Burgess Shale. Palaeogeography, Palaeoclimatology, Palaeoecology 258:222–256.

Caron, J.-B., R. R. Gaines, M. G. Mángano, M. Streng, and A. C. Daley. 2010. A New Burgess Shale-type assemblage from the "thin" Stephen Formation of the southern Canadian Rockies. Geology 38:811–814.

Chen, J. Y., L. Ramsköld, and G. Q. Zhou. 1994. Evidence for monophyly and arthropod affinity of Cambrian giant predators. Science 264:1304–1308.

Cisne, J. L. 1974. Evolution of the world fauna of aquatic free-living arthropods. Evolution 28:337–366.

Collins, D. 1996. The "evolution" of *Anomalocaris* and its classification in the arthropod class Dinocarida (Nov.) and order Radiodonta (Nov.). Journal of Paleontology 70:280–293.

Cong, P., X. Ma, X. Hou, G. D. Edgecombe, and N. J. Strausfeld. 2014. Brain structure resolves the segmental affinity of anomalocaridid appendages. Nature 513:538.

Cong, P., A. C. Daley, G. D. Edgecombe, X. Hou, and A. Chen. 2016. Morphology of the radiodontan *Lyrarapax* from the Early Cambrian Chengjiang Biota. Journal of Paleontology 90:663–671.

Cong, P., A. C. Daley, G. D. Edgecombe, and X. Hou. 2017. The functional head of the Cambrian radiodontan (stem-group Euarthropoda) *Amplectobelua symbrachiata*. BMC Evolutionary Biology 17:208.

Cong, P., G. D. Edgecombe, A. C. Daley, J. Guo, S. Pates, and X. G. Hou. 2018. New radiodonts with gnathobase-like structures from the Cambrian Chengjiang Biota and implications for the systematics of Radiodonta. Papers in Palaeontology 4:605–621.

Cong, P., Jin Guo, G. D. Edgecombe, A. C. Daley, and X. Hou. 2019. Reconstructing the feeding apparatus of Amplectobeluidae (Radiodonta: Stem Euarthropoda). Palaeontological Association 63rd Annual Meeting, Abstracts, p. 29.

Daley, A. C., and J. Bergström. 2012. The oral cone of *Anomalocaris* is not a classic "*Peytoia*." Naturwissenschaften 99:501–504.

Daley, A. C., and G. E. Budd. 2010. New anomalocaridid appendages from the Burgess Shale, Canada. Palaeontology 53:721–738.

Daley, A. C., and G. D. Edgecombe. 2014. Morphology of *Anomalocaris canadensis* from the Burgess Shale. Journal of Paleontology 88:68–91.

Daley, A. C., G. E. Budd, J.-B. Caron, G. D. Edgecombe, and D. Collins. 2009. The Burgess Shale anomalocaridid *Hurdia* and its significance for early euarthropod evolution. Science 323:1597–1600.

Daley, A. C., G. E. Budd, and J.-B. Caron. 2013a. Morphology and systematics of the anomalocaridid arthropod *Hurdia* from the Middle Cambrian of British Columbia and Utah. Journal of Systematic Palaeontology 11:743–787.

Daley, A. C., J. R. Paterson, G. D. Edgecombe, D. C. García-Bellido, and J. B. Jago. 2013b. New anatomical information on *Anomalocaris* from the Cambrian Emu Bay Shale of South Australia and a reassessment of its inferred predatory habits. Palaeontology 56:971–990.

Daley, A. C., J. B. Antcliffe, H. B. Drage, and S. Pates. 2018. Early fossil record of Euarthropoda and the Cambrian explosion. Proceedings of the National Academy of Sciences USA 115:5323–5331.

Edgecombe, G. D., S. Richter, and G. D. F. Wilson. 2003. The mandibular gnathal edges: homologous structures throughout Mandibulata? African Invertebrates 44:115–135.

Guo, J., S. Pates, P. Cong, A. C. Daley, G. D. Edgecombe, T. Chen, and X. Hou. 2018. A new radiodont (stem Euarthropoda) frontal appendage with a mosaic of characters from the Cambrian (Series 2 Stage 3) Chengjiang Biota. Papers in Palaeontology 5:99–110.

Harmon, L. J., J. T. Weir, C. D. Brock, R. E. Glor, and W. Challenger. 2008. GEIGER: investigating evolutionary radiations. Bioinformatics 24:129–131.

Haug, J. T., A. Maas, C. Haug, and D. Waloszek. 2012. Evolution of crustacean appendages. Pp. 34–73 *in* L. Watling and M. Thiel, eds. Functional morphology and diversity, 1st ed. Oxford University Press, New York.

Hou, X., J. Bergström, and P. Ahlberg. 1995. *Anomalocaris* and other large animals in the Lower Cambrian Chengjiang Fauna of southwest China. GFF 117:163–183.

Jefferies, R. P. S. 1979. The origin of chordates—a methodological essay. Pp. 443–477 *in* M. R. House, ed. The origin of the major invertebrate groups. Academic Press, London.

Karlstrom, K.E., M. T. Mohr, M. D. Schmitz, F. A. Sundberg, S. M. Rowland, R. Blakey, J. R. Foster, L. J. Crossey, C. M. Dehler, and J. W. Hagadorn. 2020. Redefining the Tonto Group of Grand Canyon and recalibrating the Cambrian time scale. Geology 48:425–430.

Kühl, G., D. E. G., Briggs, and J. Rust. 2009. A great-appendage arthropod with a radial mouth from the Lower Devonian Hunsrück Slate, Germany. Science 323:771–773.

Leander, B. S. 2008. A hierarchical view of convergent evolution in microbial eukaryotes. Journal of Eukaryotic Microbiology 55:59–68..

Lerosey-Aubril, R., and S. Pates. 2018. New suspension-feeding radiodont suggests evolution of microplanktivory in Cambrian macronekton. Nature Communications 9:3774.

Lewis, P. O. 2001. A likelihood approach to estimating phylogeny from discrete morphological character data. Systematic Biology 50:913–925.

Liu, J., R. Lerosey-Aubril, M. Steiner, J. A Dunlop, D. Shu, and J. R Paterson. 2018. Origin of raptorial feeding in juvenile euarthropods revealed by a Cambrian radiodontan. National Science Review 5:863–869.

Manton, S. M. 1964. Mandibular mechanisms and evolution of arthropods. Philosophical Transactions of the Royal Society of London B 247:1–183.

Mayers, B., C. Aria, and J.-B. Caron. 2018. Three new naraoiid species from the Burgess Shale, with a morphometric and phylogenetic reinvestigation of Naraoiidae. Palaeontology 62:19–50.

Michels, J., and S. B. Schnack-Schiel. 2005. Feeding in dominant Antarctic copepods—does the morphology of the mandibular gnathobases relate to diet? Marine Biology 146:483–495.

Moysiuk, J., and J. B. Caron. 2019. A new hurdiid radiodont from the Burgess Shale evinces the exploitation of Cambrian infaunal food sources. Proceedings of the Royal Society of London B 286:20191079.

Nanglu, K., J.-B. Caron, and R. R. Gaines. 2020. The Burgess Shale paleocommunity with new insights from Marble Canyon, British Columbia. Paleobiology 46:58–81.

Nielsen, C. 1995. Animal evolution, interrelationships of the living phyla, 1st ed. Oxford University Press, Oxford.

O'Brien, L. J., J.-B. Caron, and R. R. Gaines. 2014. Taphonomy and depositional setting of the Burgess Shale Tulip Beds, Mount Stephen, British Columbia. Palaios 29:309–324.

Olesen, J. 2007. Monophyly and phylogeny of Branchiopoda, with focus on morphology and homologies of branchiopod phyllopodous limbs. Journal of Crustacean Biology 27:165–183.

Ortega-Hernández, J., R. Janssen, and G. E. Budd. 2017. Origin and evolution of the panarthropod head—a palaeobiological and developmental perspective. Arthropod Structure and Development 46:354–379.

Pates, S., and A. C. Daley. 2017. *Caryosyntrips*: a radiodontan from the Cambrian of Spain, USA and Canada. Papers in Palaeontology 3:461–470.

Pates, S., A. C. Daley, and J. Ortega-Hernández. 2017. *Aysheaia prolata* from the Utah Wheeler Formation (Drumian, Cambrian) is a frontal appendage of the radiodontan *Stanleycaris*. Acta Palaeontologica Polonica 62:619–625.

Pates, S., A. Daley, and J. Ortega-Hernández. 2018. Response to comment on "*Aysheaia prolata* from the Utah Wheeler Formation (Drumian, Cambrian) Is a Frontal Appendage of the Radiodontan *Stanleycaris*" with the formal description of *Stanleycaris*. Acta Palaeontologica Polonica 63:105–110.

Pates, S., A. C. Daley, and N. J. Butterfield. 2019. First report of paired ventral endites in a hurdiid radiodont. Zoological Letters 5:1–11.

Rambaut A., A. J. Drummond, D. Xie, G. Baele, and M. A. Suchard 2018. Posterior summarisation in Bayesian phylogenetics using Tracer 1.7. Systematic Biology 67:901–904

R Core Team. 2020. R: a language and environment for statistical computing. R Foundation for Statistical Computing, Vienna, Austria.

Revell, L. J. 2012. Phytools: an R package for phylogenetic comparative biology (and other things). Methods in Ecology and Evolution 3:217–223.

Ronquist, F., S. Klopfstein, L. Vilhelmsen, S. Schulmeister, D. L. Murray, and A. P. Rasnitsyn. 2012a. A total-evidence approach to dating with fossils, applied to the early radiation of the Hymenoptera. Systematic Biology 61:973–999.

Ronquist, F., P. Van Der Mark, M. Teslenko, D. L. Ayres, A. Darling, S. Höhna, B. Larget, L. Liu, M. A. Suchard, and J. P. Huelsenbeck. 2012b. Mrbayes 3.2: efficient Bayesian phylogenetic inference and model choice across a large model space. Systematic Biology 61:539–542.

Rueffler, C., J. Hermisson, and G. P. Wagner. 2012. Evolution of functional specialization and division of labor. Proceedings of the National Academy of Sciences USA 109:326–335.

Smith, M. R., and J.-B. Caron. 2015. *Hallucigenia*'s head and the pharyngeal armature of early ecdysozoans. Nature 523:75.

Sun, Z., H. Zeng, and F. Zhao. 2020. A new Middle Cambrian radiodont from North China: implications for morphological disparity and spatial distribution of hurdiids. Palaeogeography, Palaeoclimatology, Palaeoecology 558:109947.

Vannier, J., C. Aria, R. S. Taylor, and J.-B. Caron. 2018. *Waptia fieldensis* Walcott, a mandibulate arthropod from the Middle Cambrian Burgess Shale. Royal Society Open Science 5(6):172206.

Van Roy, P., and D. E. G. Briggs. 2011. A giant Ordovician anomalocaridid. Nature 473:510.

Van Roy, P., A. C. Daley, and D. E. G. Briggs. 2015. Anomalocaridid trunk limb homology revealed by a giant filter-feeder with paired flaps. Nature 522:77.

Vinther, J., M. Stein, N. R. Longrich, and D. A.T. Harper. 2014. A suspension-feeding anomalocarid from the Early Cambrian. Nature 507:496.

Wang, Y. Y., D. Y. Huang, and S. X. Hu. 2013. New anomalocaridid frontal appendages from the Guanshan Biota, Eastern Yunnan. Chinese Science Bulletin 58:3937–3942.

Watling, L. 2015. Feeding and digestive system. Pp. 237–260 *in* L. Watling and M. Thiel, eds. The natural history of Crustacea: functional morphology and diversity. Oxford University Press, New York.

Whittington, H. B., and D. E. G. Briggs. 1985. The largest Cambrian animal, *Anomalocaris*, Burgess Shale, British Columbia. Philosophical Transactions of the Royal Society of London B 309:569–609.

Wills, M. A., D. E. G. Briggs, and R. A. Fortey. 1998. Evolutionary correlates of arthropod tagmosis: scrambled legs. Pp. 57–65 *in* R. A. Fortey and R. H. Thomas, eds. Arthropod relationships. Springer, Dordrecht, Netherlands.

Yang, J., J. Ortega-Hernández, S. Gerber, N. J. Butterfield, J. Hou, T. Lan, and X. Zhang. 2015. A superarmored lobopodian from the Cambrian of China and early disparity in the evolution of Onychophora. Proceedings of the National Academy of Sciences USA 112:8678–8683.

Zeng, H., F. Zhao, Z. Yin, and M. Zhu. 2018. A new radiodontan oral cone with a unique combination of anatomical features from the Early Cambrian Guanshan Lagerstätte, eastern Yunnan, South China. Journal of Paleontology 92:40–48.

Zhao, F., J.-B. Caron, D. J. Bottjer, S. Hu, Z. Yin, and M. Zhu. 2014. Diversity and species abundance patterns of the Early Cambrian (Series 2, Stage 3) Chengjiang Biota from China. Paleobiology 40:50–69.